Journal of Hazardous Materials 205–206 (2012) 101–110

Contents lists available at SciVerse ScienceDirect

Journal of Hazardous Materials

journal homepage: www.elsevier.com/locate/jhazmat

Synthesis of inorganic polymers using fly ash and primary lead slag

S. Onisei[a,b], Y. Pontikes[b,*], T. Van Gerven[c], G.N. Angelopoulos[d], T. Velea[e], V. Predica[e], P. Moldovan[a]

[a] Department of Engineering and Management for Elaboration of Metallic Materials, University Politehnica of Bucharest, Romania
[b] Department of Metallurgy and Materials Engineering, K.U. Leuven, Kasteelpark Arenberg 44, B-3001 Leuven, Belgium
[c] Department of Chemical Engineering, K.U. Leuven, W. de Croylaan 46, B-3001 Leuven, Belgium
[d] Laboratory of Materials and Metallurgy, Department of Chemical Engineering, University of Patras, Rio, Greece
[e] National Institute of Research and Development for Non-Ferrous and Rare Metals, INCDMNR-IMNR, Pantelimon, Romania

ARTICLE INFO

Article history:
Received 2 August 2011
Received in revised form
26 November 2011
Accepted 13 December 2011
Available online 23 December 2011

Keywords:
Inorganic polymer
Geopolymer
Lead slag
Microstructure
Leaching

ABSTRACT

The present work reports on the synthesis and properties of inorganic polymers ("geopolymers") made of 100% fly ash from lignite's combustion, 100% primary lead slag and mixtures of the two. In the inorganic polymers with both fly ash and lead slag the main crystalline phases detected are wüstite, magnetite, sodium zinc silicate, quartz, anorthite, and gehlenite; litharge partially dissolves. FTIR analysis in these samples revealed that the main peaks and bands of end members also exist, along with a new amorphous reaction product. In terms of microstructure, both fly ash and lead slag dissolve and contribute in the binding phase whereas the larger particles act as aggregates. For an increasing lead slag in the composition, the binding phase is changing in chemistry and reaches PbO values higher than 50 wt.% for the 100% lead slag inorganic polymer. Regarding the properties of fly ash and lead slag inorganic polymers, compressive strength is higher than 35 MPa in all cases and water absorption diminishes as the lead slag content increases. A comparison of leaching results before and after polymerisation reveals that pH is an important factor as Pb is immobilised in the binding phase, unlike Zn and As.

© 2011 Elsevier B.V. All rights reserved.

1. Introduction

Primary lead production is based on lead extraction from sulphide concentrates through a pyrometallurgical process that involves sintering, smelting in a blast furnace, drossing and refining. This process typically results in air emissions, slag, wastewaters and slurries [1,2].

The main air emissions are SO_2 and particulates. Approximately 85% of the sulphur present in the lead ore concentrate is eliminated in the sintering operation and sent to a sulphuric acid plant, about 7% is emitted as SO_2 whereas the remainder is captured by the blast furnace slag. Particulate emissions from blast furnaces are typically controlled by filters and precipitators and include a range of oxides and other metallic compounds associated with lead ores. The blast furnace slag is composed primarily of iron and silicon oxides, as well as aluminium and calcium oxides; other metals are also present in smaller amounts. This blast furnace slag is either recycled back into the process or disposed of in piles on site. This slag was retained within the Bevill exemption in the US [1] whereas in the EU the slag is considered to be a hazardous waste [3].In order to minimize the environmental footprint of the existing operations, over the past few years a hydrothermal process has been investigated in the National Institute of Research and Development for Non-Ferrous and Rare Metals, Romania (IMNR) [4]. This process replaces the high temperature oxidation step of the nonferrous metal (Cu, Pb, Zn) sulphides with a hydrothermal oxidation process. In the laboratory, this process takes place under alkaline media, moderate temperature and pressure (temperature 100 °C, pressure 6 atm, approximately) in the presence of air. Results have shown that oxidation of lead sulphide in an autoclave can reach 96% efficiency. The reaction products, principally composed of sodium lead carbonate hydroxide, are subsequently heated to reduce lead oxide. Thus, a slag is still being generated that, like the slag currently produced, may necessitate special treatment in terms of disposal. A method for the immobilisation of the leachable elements or even a valorisation scheme would be of interest.

The production of monolithic materials with lead slag is a potential option. Indeed, lead slag from secondary production has been studied for use as an aggregate or in concrete applications [5–9]. Applications in higher added-value streams, e.g. in cement production (in the raw meal or as pozzolanic/latent hydraulic material) or in heavy clay production seem unlikely due to the chemistry and mineralogy of the slag. Still, applications in harbours or in dyke fortifications may seem likely provided that the new slag produced is

* Corresponding author. Tel.: +32 16320392; fax: +32 16321991.
E-mail addresses: Yiannis.Pontikes@mtm.kuleuven.be, pontikes@gmail.com (Y. Pontikes).

0304-3894/$ – see front matter © 2011 Elsevier B.V. All rights reserved.
doi:10.1016/j.jhazmat.2011.12.039

not hazardous and that all requirements for the end-product are met.

Unlike other routes, the production of geopolymers from lead slag does not appear a priori to be impossible. Geopolymer is defined as a synthetic alkali aluminosilicate material generated from the reaction of a solid aluminosilicate with a highly concentrated aqueous alkali hydroxide or silicate solution [5,6]. These materials set and harden to an X-ray diffraction amorphous phase that contains tetrahedral Al and tetrahedral Si. Geopolymers can be considered as a subset of alkali-activated materials and inorganic polymers [7]. The latter term (inorganic polymer) is adopted in the present work to account for the deviation from aluminosilicate chemistry and possible deviation from solely tetrahedral coordination for Al and Si. A number of materials have been investigated as candidates for geopolymer/inorganic polymer production. Besides metakaolin [8], significant research has been conducted on fly ash [9–12], FeNi slag [13,14], and other high temperature residues and wastes [15,16]. The literature reported herein is not exhaustive and one can refer to relevant books [8,17,18] for further information. Despite research in this field, lead slag has not been yet tested. However, it has been demonstrated by a number of authors that Pb leaching is minimised in geopolymers [19–22], the latter being another factor advocating the present research.

In the present work, lead slag produced under laboratory conditions was mixed with alkalis and silicates and was converted to an inorganic polymer. To improve the properties, fly ash from lignite's combustion was also mixed with the lead slag. The latter was considered to be a method of supplementing the Al deficiency of lead slag.

2. Materials and methods

2.1. Materials

The lead slag was supplied by IMNR-INCDMNR (Pantelimon, Romania). It had been produced in laboratory conditions by melting oxidized lead concentrate (after the autoclave) in a resistance furnace at 1150 °C for 2 h with the addition of 3.2 wt.% coke, 5.7 wt.% SiO_2, 1.7 wt.% $Ca(OH)_2$ and 2.6 wt.% Na_2CO_3. The fly ash used was from lignite's combustion, sourced from the Megalopolis' PPC plant (Peloponnesus, Greece). Both materials used in the experiments were milled using a disc mill (Siebtechnik, Germany) below 125 μm.

The activating solution was prepared by dissolving sodium hydroxide pellets (99% NaOH) in distilled water, allowing the solution to cool at room temperature for 24 h and then mixing with sodium silicate solution (SiO_2 25.5–28.5%, Na_2O 7.5–8.5%, density 1.345–1.382 g/ml).

2.2. Analytical techniques

The chemical composition of the raw materials was determined by an X-ray fluorescence spectrometer, XRF (PW 2400 Philips). For lead slag, Co, Cu, Sb, Cr, Ni and Mn were determined by inductively coupled plasma atomic emission spectroscopy, ICP-AES (ICP Model P Spectroflame, Germany), whereas As was determined by direct-coupled plasma spectrophotometer (V DCP Spectraspan, Germany). Mineralogy of the samples was determined by X-ray powder diffraction analysis, XRD (D500 Siemens). Diffraction patterns were measured in 2θ range of 10–70° using CuKα radiation of 40 kV and 40 mA, with a 0.01° step size and step time of 3 s. Particle size distribution was analysed by laser diffraction (MasterSizer Micro Plus, Malvern). Scanning electron microscopy, SEM, combined with energy dispersive X-ray analysis, EDX (XL30 FEG, Philips) was performed on polished surfaces after carbon-coating. In selected cases, a field emission microprobe (Jeol, JXA-8530F) was employed for the microanalysis and for the generation of the elemental maps. Fourier-Transform Infrared Spectroscopy, FTIR (Spectrum BX, Perkin Elmer) spectra were collected from uniaxially pressed discs, prepared from 1 mg of powder material mixed with 150 mg analytical grade KBr. Parameters were kept for all measurements: 4400–400 cm^{-1} range, 4 numbers of scans, 4.0 cm^{-1} resolution with 1.0 cm^{-1} intervals. Chemical analysis of the leachates was performed by inductively coupled plasma mass spectroscopy, ICP-MS (XSERIES 1, Thermo Scientific).

2.3. Preparation and analysis of inorganic polymers

The methodology followed involved the preparation of 100% fly ash inorganic polymers, 100% lead slag inorganic polymers and mixtures of fly ash with lead slag, at the optimal conditions (highest compressive strength) deduced by the initial experiments.

For the one-component samples, the parameters of research were the content of sodium hydroxide, the content of sodium silicate and the curing temperature. The concentration of sodium hydroxide solution studied varied between 8 and 12 M. The high molarity of the activating solution is characteristic of fly ash geopolymers [17]. The preparation of the samples involved mixing the powders with the activating solutions for approximately 4 min in a high rpm/torque bench mixer and pouring the product into rectangular moulds (80 mm × 20 mm × 20 mm). The free surface was covered with cling film and the samples were left for curing at 20 °C in an air-conditioned room or at 70 °C in a drying kiln. After 24 h the samples were de-moulded, wrapped in cling film, and left to cure for 28 days more. Compressive strength tests (Model 8872, Instron) on samples 20 mm × 20 mm × 20 mm, with a head displacement rate of 1 mm/min, were performed to evaluate the one-component samples.

The two-component samples were prepared in a procedure similar to the one described above. Four mixtures were studied, with the lead slag content in wt.% (vol.% in parenthesis): 28 (20), 51 (40), 70 (60) and 86 (80). The samples are denoted as GLS28, GLS51, GLS70 and GLS86. GLS0 and GLS100 denote 100% fly ash and 100% lead slag inorganic polymers, respectively. The activating solution for the two-component samples is described in Eq (1):

$$\begin{bmatrix} SS \\ SH \end{bmatrix}_{Set\ III} = (1 - wt.\%\ lead\ slag) \times \begin{bmatrix} SS \\ SH \end{bmatrix}_{Set\ I} + (wt.\%\ lead\ slag) \times \begin{bmatrix} SS \\ SH \end{bmatrix}_{Set\ II} \quad (1)$$

where SS: sodium silicate (solution, SiO_2 25.5–28.5%, Na_2O 7.5–8.5%), SH: sodium hydroxide (solution, 12 M), Set I: inorganic polymers with fly ash, Set II: inorganic polymers with lead slag, Set III: inorganic polymers with fly ash and lead slag. The conditions for set I and set II correspond to the highest compressive strength obtained. The curing temperature was 20 °C approximately. Table 1 summarises the design parameters of all samples.

The microstructure of the resulting inorganic polymers was analysed by XRD, FTIR and SEM. The open porosity and bulk density were measured according to ASTM C20-00. Mechanical properties were measured in a 3-point configuration for flexural (sample of 80 mm × 20 mm × 20 mm) and "in compression" mode (sample of 20 mm × 20 mm × 20 mm), with a head displacement rate of 1 mm/min in both cases (Model 8872, Instron).

The leaching experiments were conducted on two materials: the inorganic polymer exhibiting the highest compressive strength (assuming optimal polymerisation) and a mixture of (raw) powders of fly ash and lead slag in the same ratio as in the chosen inorganic polymer. All samples were milled < 125 μm and their

Table 1
Synthesis conditions for the mixtures of fly ash and lead slag. SS: sodium silicate (solution, SiO_2 25.5–28.5%, Na_2O 7.5–8.5%), SH: sodium hydroxide (solution, 12 M), *S*/*L*: solid inorganic polymer precursor to liquid solutions, Si/Al: silica to alumina ratio (total values, including raw materials and solution added).

Oxide	Fly ash	Lead slag
SiO_2	51.44	21.56
Al_2O_3	23.52	1.73
Fe_2O_3	7.73	31.57
CaO	9.21	3.05
MgO	1.69	0.15
Na_2O	0.89	13.02
K_2O	1.45	0.26
SO_3	2.66	8.01
PbO	<0.01	12.28
ZnO	<0.01	6.18
As_2O_3	n.d.	0.20
CoO	n.d.	0.02
Cr_2O_3	n.d.	0.35
CuO	n.d.	1.64
MnO	n.d.	0.10
NiO	n.d.	<0.01
Sb_2O_3	n.d.	0.26

particle size distribution was analysed by laser diffraction. The solids were mixed with deionised water in a 1:10 ratio and 65% HNO_3 was added in order to reach pH values ranging from 5 to 12 approximately. The solutions were kept for 24 h in a shaking table and the pH measurement was taken at the leachate after filtering through a 0.45 μm filter. The pH is not controlled over the 24 h duration of the experiment. The procedure is based on the EN12457 leaching test standard and is explained in more detail in Kosson et al. [23].

3. Results and discussion

3.1. Raw materials

The fly ash, Table 2, used for the experiments is classified as type F according to ASTM C-618 [24]; the total content in SiO_2, Al_2O_3 and Fe_2O_3 is higher than 70 wt.% whereas CaO is 9.2 wt.%. Lead slag, Table 2, has a high content of Fe_2O_3, SiO_2, Na_2O and PbO whereas is very poor in Al_2O_3 (1.73 wt.%). Sulphur and ZnO content are also substantial whereas in smaller quantities contains As, Co, Cr, Cu, Mn and Sb. The high level of Pb is due to the non-optimised laboratory conditions during lead oxide reduction.

Fly ash is significantly finer, already in the as-received state, compared to lead slag, Fig. 1. The mean particle size (d_{50}) for fly ash is 4.4 μm whereas for lead slag it is 37.1 μm. Despite sieving below 125 μm, a portion of the lead slag appears to be higher than 200 μm in the laser analysis, probably due to particle morphology.

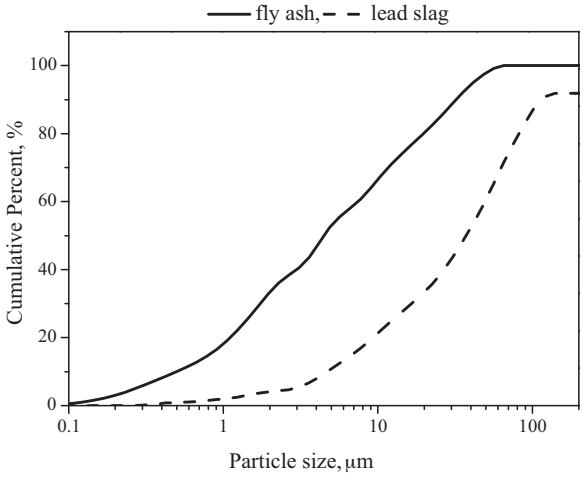

Fig. 1. Particle size distribution analysis of fly ash and lead slag.

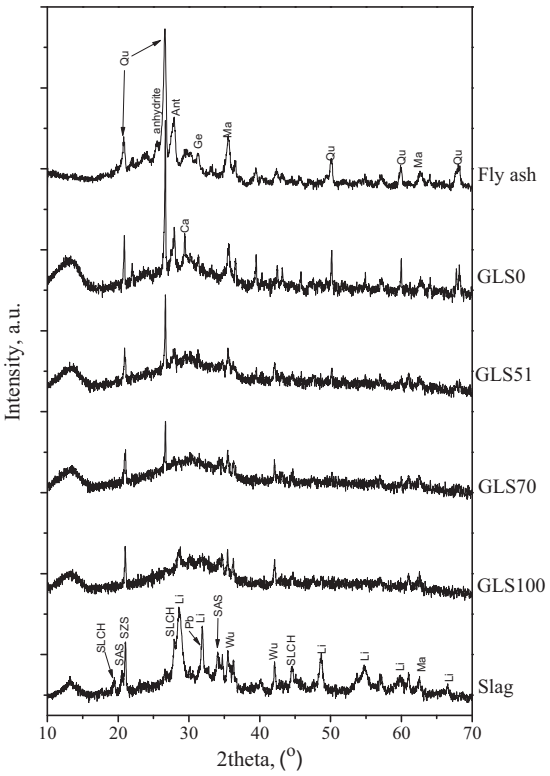

Fig. 2. X-ray diffractograms for raw materials and inorganic polymers with different quantities of slag. Label: symbol in figure-mineral (PDF number from ICDD). Qu-quartz (461-045), An-anorthite (411-486), Ma-magnetite (19-629), Ge-gehlenite (35-755), Ca-calcite (5-586), Li-litharge (5-561), SAS-sodium aluminium silicate (11-221), Wu- wüstite (6-615), SZS-sodium zinc silicate (37-407), Pb-lead (23-345).

The main phases in fly ash are quartz (SiO_2), anorthite ($CaAl_2Si_2O_8$), magnetite (Fe_3O_4), anhydrite ($CaSO_4$) and gehlenite ($Ca_2Al_2SiO_7$), Fig. 2 also for PDF numbers from the ICDD. For lead slag, the main phases detected are litharge (PbO), sodium aluminium silicate ($Na_6Al_4Si_4O_{17}$), wüstite (FeO), magnetite (Fe_3O_4), sodium zinc silicate (Na_2ZnSiO_4) sodium lead carbonate hydroxide ($NaPb_2(CO_3)_2OH$) and possibly lead (Pb). Sodium lead carbonate hydroxide appears during storage of the lead slag.

3.2. Synthesis of inorganic polymers

3.2.1. Inorganic polymers with 100% fly ash and 100% lead slag

For the GLS0, the highest compressive strength was 50 ± 9 MPa, obtained for the samples with ratios *S*/*L* 1.77, Si/Al 4.43 and curing temperature 70 °C. The overall Si/Al ratios reported here and later on for the other formulations studied, are more indicative than representative of the polymer chemistry as there will be incomplete reaction of the solid particles. Microchemical analysis of the binding phase (Section 3.3.3) sheds more light.

For the GLS100, the most significant obstacle encountered was the formation of cracks during curing. The problem was ascribed to shrinkage and/or low cohesion in the paste. In order to minimize it, the curing temperature was decreased from 70 °C to 20 °C and *S*/*L* ratio was increased as much as the rheology of the system permitted for casting. The highest compressive strength obtained was 30 ± 8 MPa, for *S*/*L* 4.94, Si/Al 26.41 and curing at room temperature. The ratio of Si/Al is rather high compared to most geopolymer formulations in the literature, however, this factor is not necessarily precluding the formation of a well developed cross-linked

Table 2
Chemical composition of fly ash and lead slag, in wt.%, n.d.: not determined.

Mixture	Inorganic polymer precursor		SS, wt.% of inorganic polymer precursor	SH, wt.% of inorganic polymer precursor	*S*/*L*	Si/Al
	Fly ash wt.%	Slag wt.%				
GLS0	100	0	29.4	26.9	1.77	4.43
GLS28	71.8	28.2	25.4	20.8	2.16	5.04
GLS51	48.9	51.1	22.0	15.7	2.65	5.97
GLS70	29.8	70.2	19.4	11.5	3.23	7.63
GLS86	13.8	86.2	17.2	8.0	3.97	11.30
GLS100	0	100	15.3	5.0	4.94	26.41

network. Indeed, other authors have demonstrated that compositions of SiO_2/Al_2O_3 between 2 and 300 showed typical amorphous geopolymer XRD traces and ^{27}Al, ^{29}Si and ^{23}Na NMR spectra [25].

3.2.2. Inorganic polymers of fly ash and lead slag

As reported in Table 1, the inorganic polymers with fly ash and lead slag had values of *S*/*L* ranging from 2.16 to 3.97 and Si/Al ranging from 5.04 to 11.30.

3.3. Properties of inorganic polymers

3.3.1. Crystalline phases

For GLS0, the major phases detected are quartz, anorthite, magnetite and gehlenite; results, including the PDF numbers of the phases from the ICDD, are presented in Fig. 2. Other authors have also noted the dissolution of anhydrite in alkaline environments for a comparable fly ash [26,27]; it is possible that anhydrite transforms first to gypsum and then gypsum dissolves in the alkaline solution [28]. A new phase identified at $2\theta = 29.45^\circ$ is most probably calcite, resulting after the carbonation of free CaO originating from anhydrite. Other authors [9] have demonstrated the importance of curing conditions on the carbonation. As the samples were placed at a relative low humidity, and not in air-tight containers, it is not surprising that calcite has been formed. The formation of sodium carbonate or sodium bicarbonate in small amounts cannot be excluded either, as weak peaks appear between $2\theta = 30.05^\circ$ and 30.35°. Other new phases were not detected, despite the fact that many authors observe the formation of zeolites [29,30]. The main reason for this is probably the lower curing temperature and curing duration [29]. Moreover, although it is generally found [9,27] that the broad hump indicative of the amorphous phase slightly shifts to higher values, i.e. originally from $2\theta = 20–30^\circ$ to $2\theta = 25–40^\circ$ in fly ash inorganic polymers, such a change is difficult to confirm.

Regarding GLS100, the addition of alkalis had a more intense impact, Fig. 2. The identified phases are sodium zinc silicate, wüstite and magnetite as well as weak reflections of litharge. The dissolution of litharge was expected due to the amphoteric character of PbO and creates an interesting case with regards to subsequent leaching behaviour.

In the inorganic polymers formed with fly ash and lead slag, no new phases were detected and the intensity of XRD reflections appeared to be in accordance with the ratio of fly ash to lead slag.

3.3.2. Bond characteristics

As the inorganic polymer is typically XRD-amorphous, infrared spectroscopy was employed as an analytical technique in order to elucidate more the occurring reactions. Already, significant research work on infrared spectroscopy for fly ash geopolymers has been reported [12,27,31,32].

The IR spectrum of the fly ash contains five main wide and intense bands (Fig. 3) from (approximately) 430 cm^{-1} to 500 cm^{-1}, 800 cm^{-1} to 1300 cm^{-1}, 1350 to 1550 cm^{-1}, 1550 to 1740 cm^{-1} and 3000 cm^{-1} to 3700 cm^{-1}. The first band peaks at 460 cm^{-1} and corresponds to T—O (T = Al, Si) bending vibrations [31,33]. The second band has a peak at 1083 cm^{-1} and is associated with T—O bond asymmetric stretching vibrations [31,33]. The band with a peak at 1445 cm^{-1} is due to stretching vibrations of O—C—O and indicates the presence of carbonates, possibly traces of calcite, whereas the bands around 1635 cm^{-1} and 3500 cm^{-1} are ascribed to stretching (—OH) and bending (H—O—H) vibrations of bound water molecules [27]. The presence of quartz is responsible for a series of bands with peaks located at 460, 517, 668, 695, 779, 797, 1082 and 1150–1165 cm^{-1} (last two peaks not clear) [31,34]. Regarding plagioclase (probably anorthite) and gehlenite, a large number of characteristic peaks falls within the wide band from 800 cm^{-1} to 1300 cm^{-1} however peaks are identified at 668 cm^{-1} and 575 cm^{-1} for anorthite and 720 cm^{-1} for gehlenite [35,36].

Concerning the changes that took place in the fly ash after polymerisation, the first observation is that the band attributed to the asymmetric stretching vibrations of Si–O–Si and Al–O–Si at 1085 cm^{-1} becomes sharper and shifts to lower frequencies (approx. 1005 cm^{-1}) indicating the formation of a new product, the amorphous aluminosilicate phase [27]. The band located at about 460 cm^{-1}, associated to Si—O—Si and O—Si—O, is slightly decreased which indicates that quartz partially dissolves in the strong alkaline solution. Contrary to this, the band at 1445 cm^{-1} is more intense, possibly due to the formation of sodium bicarbonate and/or calcite,

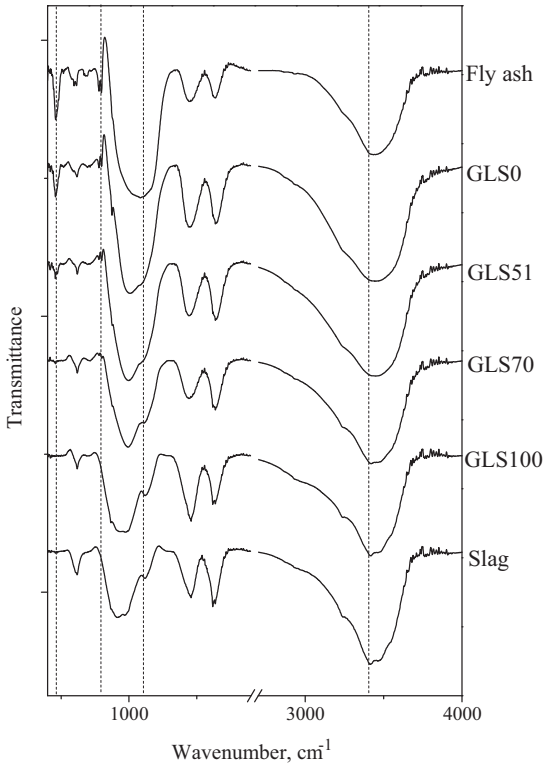

Fig. 3. IR characteristic bands for raw materials and inorganic polymers with different quantities of lead slag.

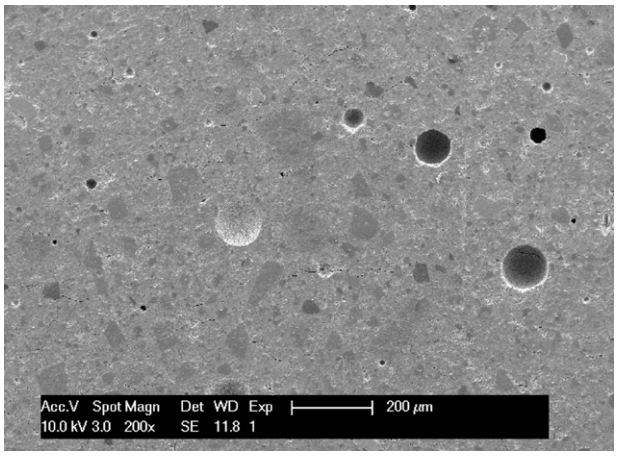

Fig. 4. Microstructure for 51 wt.% lead slag inorganic polymers.

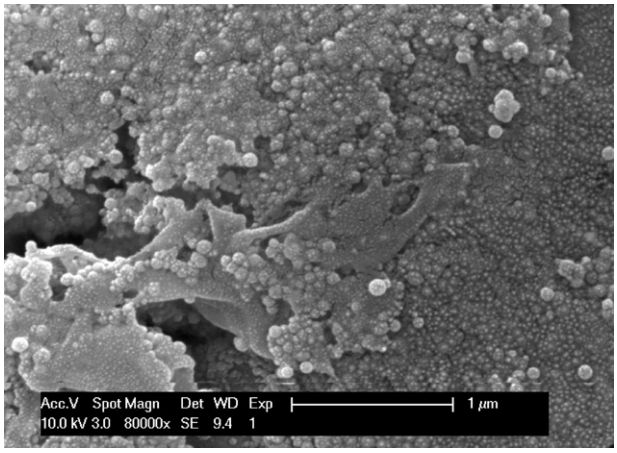

Fig. 5. Matrix for 51 wt.% lead slag inorganic polymers.

and similarly, the band around 3500 cm^{-1} is also stronger, suggesting a higher degree of water molecules' retention in the mass. Another change which is in accordance with the X-ray diffraction analysis is the detection of a small peak at 877 cm^{-1} that is believed to correspond to calcite [34].

The overview of IR spectra of lead slag resembles that of a fly ash containing five wide and intense bands (Fig. 3). However, the respective wave numbers and the intensity differ and in some cases, smaller peaks can be clearly seen in a broader band. The first band peaks at 620 cm^{-1} and is attributed to the presence of sulphate ions [37]. A second band appears between 760 cm^{-1} and 1220 cm^{-1}, with peaks at 868 cm^{-1}, 914 cm^{-1}, 972 cm^{-1} and 1119 cm^{-1}. Already ascribed to T—O bond asymmetric stretching vibrations, it is interesting to note the shift to smaller wavenumbers as compared to the respective band in fly ash. This is attributed to the length as well as angle of the Si—O and Al—O bonds in the silicates, in this case being sodium aluminium silicate, sodium zinc silicate and probably also other XRD-amorphous silicate phases. Three more bands appear between 1340 cm^{-1} and 1540 cm^{-1}, 1540 cm^{-1} and 1740 cm^{-1} and a diffuse one that peaks at 3410 cm^{-1}. In line with previous analysis, these are due to stretching vibrations of O—C—O (1340 cm^{-1} and 1540 cm^{-1}) and stretching (—OH) and bending (H—O—H) vibrations of bound water molecules (1635 cm^{-1} and 3500 cm^{-1}, respectively). The presence of the crystalline phases, as detected by XRD, is difficult to confirm as only weak absorption bands appear and there is limited available information for the identified silicates. Nonetheless, the characteristic peaks of litharge at 460 cm^{-1} [38] and wüstite at 425 cm^{-1} [39] are indeed present. The presence of magnetite cannot be confirmed as its strong peak at 580 cm^{-1} falls in the first band [39].

In the GLS100 inorganic polymers, the FTIR spectrum appears almost identical to the raw material. Nonetheless, the small absorption band of litharge does disappear, which confirms the XRD results, and the band caused by the stretching vibrations of O—C—O is enhanced due to increased carbonation.

Concerning the inorganic polymers with both fly ash and lead slag, a similar trend to the one found in XRD patterns is observed: as the percent of lead slag in the body increases, the IR spectra resemble more the 100% lead slag inorganic polymer. Also in this case, no interaction between the two end members is detected.

3.3.3. Microstructure

The microstructure of GLS51, Fig. 4, is comprised of large grains, typically between 50 μm and 100 μm, embedded in a matrix. The larger grains are typically angular and show good adherence to the matrix. The matrix is presented in Fig. 5, where sub-micron particles of spherical morphology, probably partially dissolved fly ash, are bounded by the polymeric reaction product. Spherical pores caused by trapped air are also observed as well as a small number of cracks. As the lead slag content increases, the fly ash relics cease to appear. No cracks were visible, Fig. 6, for GLS70.

Analyses for GLS70 by EDX, Fig. 6, and WDS elemental mapping, Fig. 7, provide greater insight into the microstructure. The larger grains in the samples derive mostly from the lead slag and are amorphous. These grains are not homogeneous; some contain clusters of Cr-bearing spinels, are devitrified or contain various inclusions such as iron oxide or metallic Pb. The average chemistry of 10 different grains on the glassy part is: Na_2O: 29.84 ± 2.85, Al_2O_3: 4.36 ± 1.09, SiO_2: 42.53 ± 4.97, SO_3: 10.05 ± 2.75, CaO: 2.93 ± 1.00, FeO: 10.71 ± 5.37. The sulphur content, higher than the reported studies in terms of S solubility for sodium silicate glasses [40], is most likely an artefact in the analyses. The most plausible hypothesis is that results include a S-rich separated phase, such as Na_2SO_4, or S-rich inclusions, Fig. 7. Fe exists in well defined areas as iron oxides and metallic Fe, in association with spinels and in the amorphous phase. Lead is mostly found in the binding phase, Fig. 7. Metallic Pb and PbO were found as inclusions in larger grains whereas Pb-rich micro-sites were also detected. In addition to the amorphous phase, Si is also found in small grains of SiO_2, probably quartz, as well as in anorthite and gehlenite along with Al and Ca.

The microstructure of GLS100 is comprised of grains with a variable size and morphology, a clearly discernible binding phase and a considerable presence of cracks, Fig. 8. EDX microanalysis enabled the determination of the chemistry of the binding phase and the

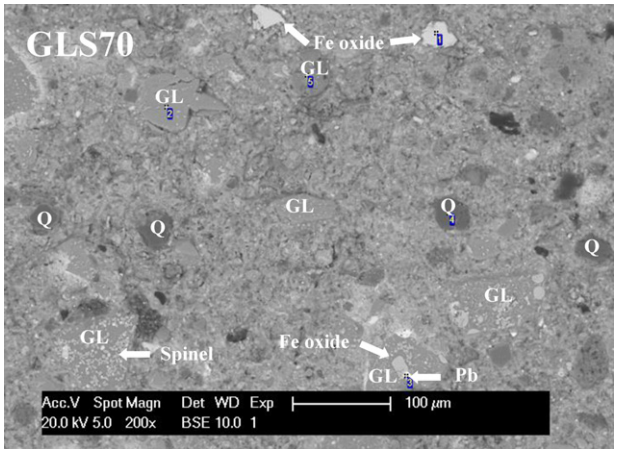

Fig. 6. Microstructure for 70 wt.% lead slag inorganic polymers. GL: glass, Q: quartz, Fe oxide: wüstite/magnetite, Pb: lead.

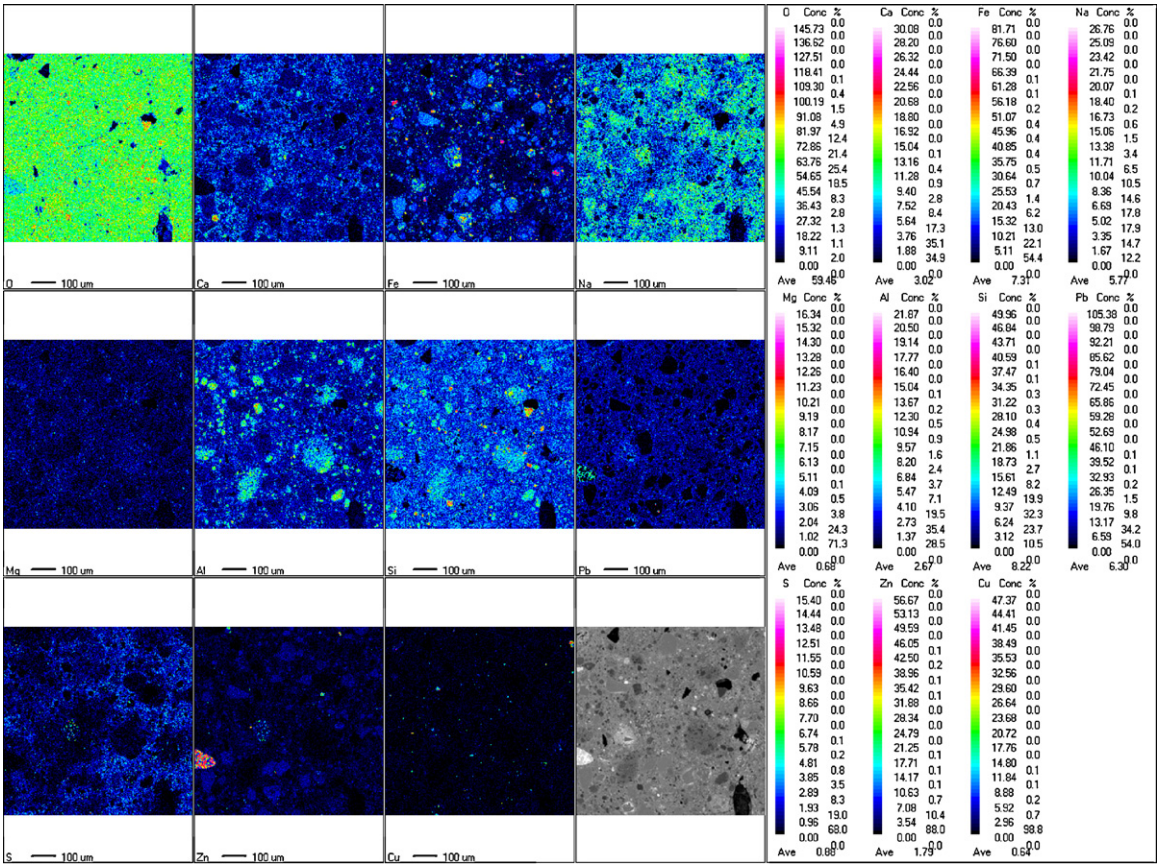

Fig. 7. WDS elemental mapping for 70 wt.% lead slag inorganic polymers; values for oxygen indicative.

results are summarised in Table 3 for a number of selected points. It results that the binding phase contains, on an average, more than 50 wt.% PbO, with also relative high levels of FeO, SiO_2 and ZnO. The average Si/Al ratio is approximately 33. Considering the high content of Pb content in the binding phase, the inorganic polymer developed herein may be seen as an analogue to lead silicate glasses.

3.3.4. Physical properties

Flexural strength is comparable in all cases, ranging from 2.2 ± 0.3 MPa to 2.8 ± 0.1 MPa, Fig. 9. Regarding compressive strength, there is a clear gain observed, at least up to 70 wt.% lead slag addition. Higher lead slag content leads to a decrease in compressive strength, from 47 ± 4 MPa (for GLS70), to approximately 35 ± 5 MPa for GLS86.

A discussion on how lead slag addition affects the mechanical properties would have to acknowledge that each inorganic polymer studied has been made with a different activating solution. Even if a clear focus on the effect of lead slag itself is not possible, some general mechanisms can still be deduced. Based on SEM analysis, it has been demonstrated that lead slag particles mainly behave as aggregates. Nonetheless, other factors such as the surface area for interfacial chemical bonding between the binding phase and the aggregate, the nature of the chemical bond itself and the dissolution behaviour of the particular mixture of solid precursor/aggregate in the activating solution [41] should be considered. Indeed, the analysis on the binding phase revealed clear differences in terms of chemistry. Another factor influencing the compressive strength is porosity. As presented in Fig. 10, open porosity (water absorption) decreases with an increase in lead slag content. However, considering the absence of any data pertinent to pores' size distribution or closed porosity, no definite conclusion can be drawn.

Bulk density and water absorption increase and decrease respectively with lead slag addition, Fig. 10. Obviously, the change in bulk density is attributed to the higher density values of lead slag, which results in a figure of 2.23 g/cm^3 for GLS86. The decrease

Table 3
EDS results on the GLS100 binding phase, with average values and standard deviation (St. Dev).

													Average	St. Dev.
SiO_2	11.27	13.49	11.63	11.93	12.11	10.25	11.82	13.17	12.42	12.18	13.91	12.72	12.24	1.00
Al_2O_3	0.48	0.71	0.59	0.53	0.69	0.41	0.67	0.78	0.78	0.63	0.85	0.68	0.65	0.13
FeO	19.58	17.23	24.01	15.99	17.03	12.30	16.53	18.35	24.42	23.15	21.48	14.52	18.72	3.87
CaO	2.62	3.97	3.14	2.26	3.26	2.64	2.59	3.51	4.69	2.80	3.51	3.23	3.19	0.68
MgO	0.36	0.54	0.49	0.16	0.33	0.17	0.15	0.43	0.28	0.08	0.53	0.32	0.32	0.16
Na_2O	2.65	4.83	4.84	2.90	3.47	2.34	2.12	4.62	3.15	3.05	5.12	2.85	3.50	1.07
SO_3	2.15	2.40	2.67	0.66	3.20	0.00	0.00	2.06	2.97	1.51	2.10	0.66	1.70	1.12
PbO	52.74	49.35	45.26	57.61	51.54	66.05	59.11	48.81	42.25	48.73	44.42	57.92	51.98	7.01
ZnO	6.22	6.70	5.93	5.92	6.93	5.39	5.65	6.25	7.06	6.79	7.21	5.57	6.30	0.62
CuO	1.92	0.77	1.44	2.05	1.43	0.45	1.37	1.92	1.98	1.35	0.86	1.54	1.42	0.51

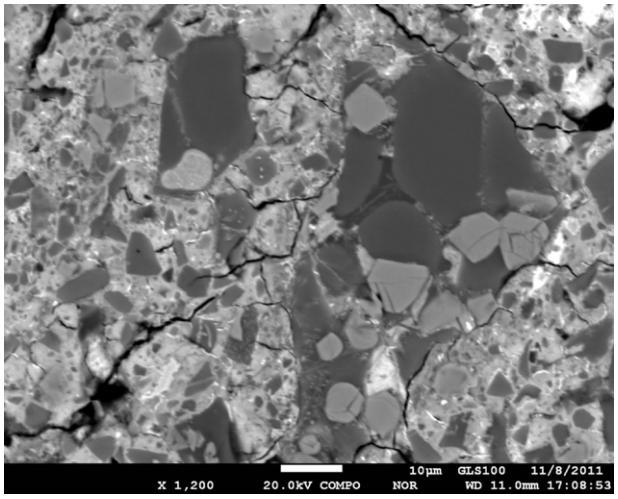

Fig. 8. Microstructure for 100 wt.% lead slag inorganic polymers.

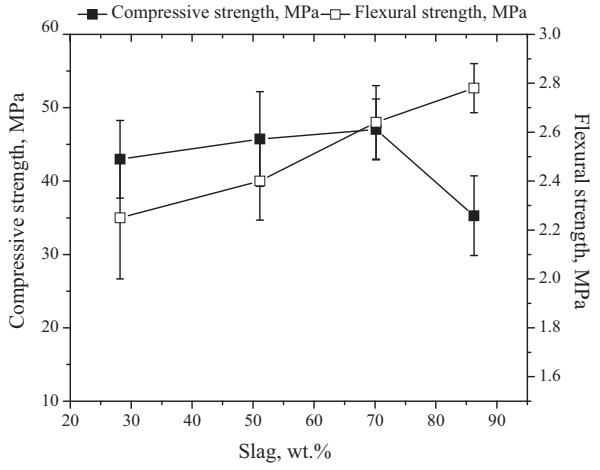

Fig. 9. Flexural and compressive strength for inorganic polymers with different lead slag content.

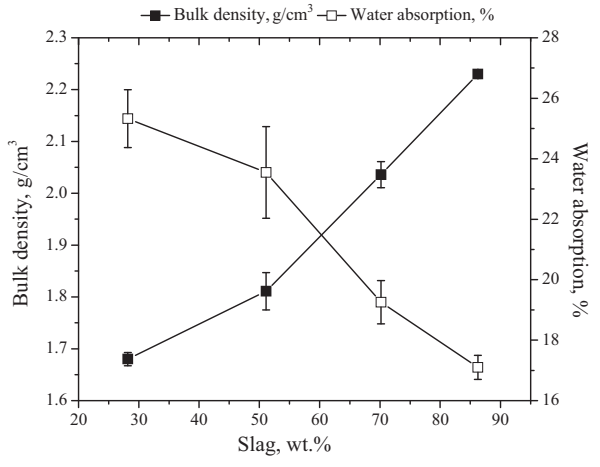

Fig. 10. Water absorption and density for inorganic polymers with different lead slag content.

in water absorption, however, with an increase in lead slag content is an interesting result, considering that lead slag is less reactive. From a value of 25.4 ± 0.9% for GLS28, there is continuous reduction as lead slag increases, reaching a value of 17.1 ± 0.4% for GLS86.

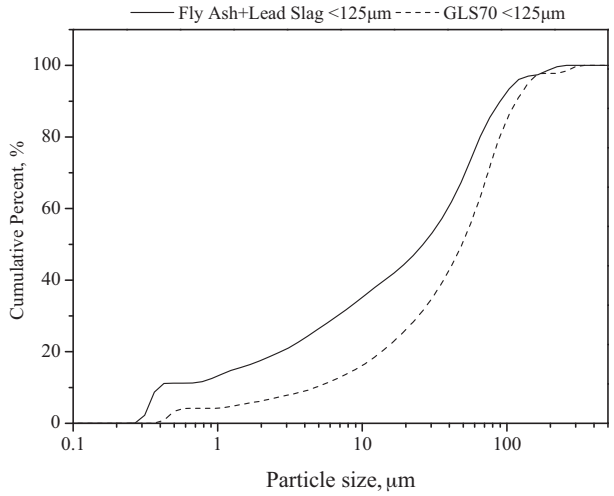

Fig. 11. Particle size distribution (after milling below 125 μm) of fly ash and lead slag precursor and inorganic polymer GLS70.

This behaviour could be related to improved particle packing and/or avoidance of areas with micro-porosity, as they appear in Fig. 5.

3.3.5. Leaching

Leaching analysis was conducted on a mixture of fly ash/lead slag 30:70 and the corresponding inorganic polymer, GLS70. The particle size distribution of the two materials, Fig. 11, shows that the mixture of fly ash and lead slag is finer, thus, of higher surface. The particular protocol that was followed permitted the monitoring of leachable elements as a function of pH, Fig. 12. In most work related to inorganic polymer leaching the role of pH has not been a focus point although notable exceptions do exist [42]. However, as results reveal, the influence of pH often proved to be fundamental, with variations of up to 4 times in magnitude. The starting pH of fly ash/lead slag mixture and inorganic polymer in the solution was 12.3 and 12.5, respectively.

In more detail, results demonstrate low leaching for Si. Higher values are recorded for the inorganic polymer, but even for the worst case scenario tested of pH approximately 12.5, Si leaching is below 60 ppm. Based also on the results from microchemical analysis, it is evident that the activating solution (rich in Si) promotes the dissolution of solid precursors, resulting in a new water-insoluble binding phase.

Polymerisation was beneficial in immobilising Pb. Comparing the results before and after polymerisation it is evident that in the approximate range of pH 6–8, the concentration of lead in solution decreased up to 2.4 times and in the approximate range of pH 11–12, the concentration was reduced up to 5.3 times. These results are in accordance with reported work [19–22], as was summarised in the introduction. Regarding the nature of the immobilisation, it is suggested that Pb may be incorporated either in the amorphous aluminosilicate structure [22,43], or crystallise towards Pb_3SiO_5 [20] or Na_6PbO_5 [13], depending on the precursor and synthesis conditions. Based on mass calculations and the elemental maps of Fig. 8 the formation of such crystalline products appears unlikely in the present system. The Pb content for Pb_3SiO_5 should be approximately 85.2 wt.% whereas for Na_6PbO_5 should be approximately 48.7 wt.%. However, the elemental map of Pb shows that 99.5% of the selected area has a Pb content below 26.35 wt.%. There is practically no area (other than PbO and metallic Pb) with the high concentration expected for Pb_3SiO_5 and Na_6PbO_5.

For Al, a network-forming element in the inorganic polymer matrix, the results are comparable to Pb behaviour. Polymerisation immobilised the element in the alkaline region (from pH 9 to

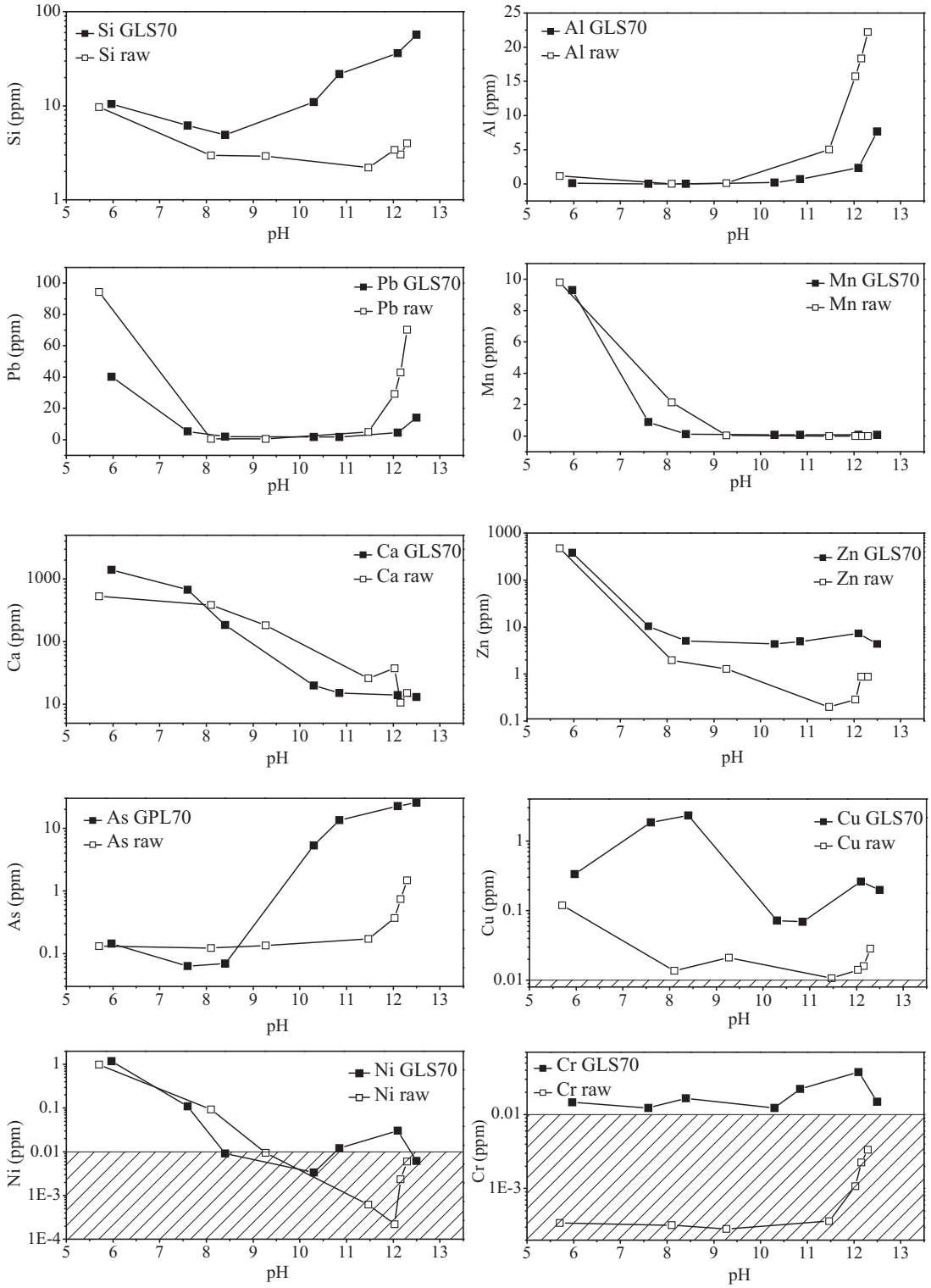

Fig. 12. Leaching behaviour of selected elements as a function of pH, before (raw) and after polymerisation (GLS70); details for the particle size distribution are presented in Fig. 11.

12 approximately) whereas in the neutral region, down to pH 6, the released Al from inorganic polymers or the raw mixture was below 2.5 ppm.

Mn is barely affected, the differences being in the range of ppm. Ca on the other hand, for pH between 6 and 8, becomes more soluble after polymerisation, whereas leaching is minimised for higher values, up to pH 12. Other authors have also found that polymerisation is beneficial for Ca immobilisation in fly ashes at high pH [44]. The lower mobility could be ascribed to the formation of $CaCO_3$ or $CaSO_4$.

Regarding Zn, polymerisation did not have a significant influence from pH 6 to pH 8 but had a negative influence for a pH range of

8–12, where the concentration of Zn in solution increased approximately 5 times. Higher release of Zn after polymerisation, compared to the raw materials, has been reported before in fly ashes [44]. In the present case, Zn arose predominantly from the Zn-bearing phases in lead slag, such as sodium zinc silicate. Apparently, during polymerisation, the high alkalinity promoted the dissolution of such phases, possibly in a mechanism similar to that reported for zinc silicates [45]. Indeed, the elemental mapping of Fig. 8 and the results of Table 3 corroborate for the dissolution of Zn and its participation in the binding phase. This suggestion does not contradict the apparent lack of change in terms of XRD peaks for sodium zinc silicate in Fig. 2. Zn leaching is in the range of 10 ppm and only a limited transformation of sodium zinc silicate, not amendable to XRD analysis, would suffice.

For As, the released quantity increased by one order of magnitude, i.e. to 25 ppm, compared to the raw materials when the pH was higher than 8.5. Other authors observed similar behaviour [44] whereas it is possible that the concentration and chemical form of iron in the aqueous phase, related to As immobilisation [46], may have an impact on the results. Similarly, for Cu, there is increased leaching after polymerisation, even if the values always remain <3 ppm. Previous results also verify that Cu immobilisation is not as efficient as Pb [21,47].

Ni, Cr and Sn (results not presented for Sn; always below 0.02 ppm) exhibit very low concentrations, below or very close to the detection limit (shaded area in graph below 0.01 ppm), and the impact of polymerisation is not evident.

Thus, summarising the results, 4 clusters can be identified: a decrease of leaching capacity (Pb, Al), a limited change that depends on pH (Ca, Mn), an increase of leaching capacity (Zn, As, Cu) and results very close to the detection limit (Ni, Sn, Cr).

4. Conclusions

The properties of inorganic polymers made of fly ash agree with published data. For the inorganic polymers with lead slag, the binding phase contains, on an average, more than 50 wt.% PbO, with also relative high levels of Fe, Si and Zn; the average Si/Al ratio is approximately 33. Despite crack formation, the mechanical properties were acceptable. To overcome the Al-deficiency, inorganic polymers of fly ash and lead slag were developed.

In the inorganic polymers formed with fly ash and lead slag, the main change occurring after polymerisation was the formation of a new amorphous reaction product. The dissolution of selected phases, such as litharge, sodium lead carbonate hydroxide, sodium aluminium silicate and calcium sulphate was also detected.

The microstructure of the inorganic polymers with fly ash and lead slag comprised of angular glass particles, mostly from the lead slag, with sizes typically between 50 μm and 100 μm, and a binding phase mainly rich in Si, Fe, Na and Pb, depending on the particular mix. Porosity exists as micro-porosity in regions rich in fly ash and as closed spherical pores due to air entrapment.

For the fly ash and lead slag inorganic polymers produced, water absorption was lower than 26% and compressive strength was higher than 35 MPa. For the inorganic polymers made of 70 wt.% lead slag and 30 wt.% fly ash, the water absorption was $19.3 \pm 0.7\%$ and the compressive strength was 47 ± 4 MPa.

A comparison of leaching results, before and after polymerisation, demonstrates a decrease of leaching for Pb and an increase of leaching for Zn and As. The influence of pH is substantial in selected cases.

Acknowledgements

SO is thankful to the State Scholarship Foundation of Greece for the financial support she received during her PhD studies. YP is thankful to the Research Foundation – Flanders for the post-doctoral fellowship.

References

[1] U.S. Environmental Protection Agency, Profile of the Nonferrous Metals Industry, in, EPA/310-R-95-010, Office of Compliance, Office of Enforcement and Compliance Assurance, U.S. Environmental Protection Agency, Washington, DC, 1995.
[2] Institute for Prospective Technological Studies, Joint Research Centre, Reference document on best available techniques in the non ferrous metals industries, in: Integrated Pollution Prevention and Control (IPPC) (Ed.), Sustainability in Industry, Energy and Transport, European IPPC Bureau, European Commission, 2001.
[3] Office for Official Publications of the European Communities, European waste catalogue and hazardous waste list in: Environmental Protection Agency (Ed.), Ireland, 2002.
[4] S. Onisei, On the oxidation of non-ferrous metal sulphides under pressure and alkali activation of the resulting slag for the production of building materials. PhD dissertation, in, Polytechnic University of Bucharest, Bucharest, 2011 (expected).
[5] J. Davidovits, Geopolymers, J. Therm. Anal. Calorim. 37 (1991) 1633–1656.
[6] P. Duxson, A. Fernández-Jiménez, J.L. Provis, G.C. Lukey, A. Palomo, J.S.J. Van Deventer, Geopolymer technology: the current state of the art, J. Mater. Sci. 42 (2007) 2917–2933.
[7] J. van Deventer, J. Provis, P. Duxson, D. Brice, Chemical research and climate change as drivers in the commercial adoption of alkali activated materials, Waste and Biomass Valorization 1 (2010) 145–155.
[8] J. Davidovits, Geopolymer Chemistry and Applications, Geopolymer Institute, 2008.
[9] M. Criado, A. Fernández-Jiménez, A. Palomo, Alkali activation of fly ash. Part III: effect of curing conditions on reaction and its graphical description, Fuel 89 (2010) 3185–3192.
[10] A. Fernández-Jiménez, A. Palomo, Characterisation of fly ashes. Potential reactivity as alkaline cements, Fuel 82 (2003) 2259–2265.
[11] G. Kovalchuk, A. Fernández-Jiménez, A. Palomo, Alkali-activated fly ash: effect of thermal curing conditions on mechanical and microstructural development – Part II, Fuel 86 (2007) 315–322.
[12] C.A. Rees, J.L. Provis, G.C. Lukey, J.S.J. van Deventer, In situ ATR-FTIR study of the early stages of fly ash geopolymer gel formation, Langmuir 23 (2007) 9076–9082.
[13] K. Komnitsas, D. Zaharaki, V. Perdikatsis, Geopolymerisation of low calcium ferronickel slags, J. Mater. Sci. 42 (2007) 3073–3082.
[14] I. Maragkos, I.P. Giannopoulou, D. Panias, Synthesis of ferronickel slag-based geopolymers, Miner. Eng. 22 (2009) 196–203.
[15] I. Kourti, D.A. Rani, D. Deegan, A.R. Boccaccini, C.R. Cheeseman, Production of geopolymers using glass produced from DC plasma treatment of air pollution control (APC) residues, J. Hazard. Mater. 176 (2010) 704–709.
[16] S. Kumar, R. Kumar, S. Mehrotra, Influence of granulated blast furnace slag on the reaction, structure and properties of fly ash based geopolymer, J. Mater. Sci. 45 (2010) 607–615.
[17] J.L. Provis, J.S.J. van Deventer, Geopolymers: structures, processing, properties and industrial applications, Woodhead Publishing Ltd., 2009.
[18] C. Shi, D. Roy, P. Krivenko, Alkali-activated Cements and Concretes, Spon Press, 2006.
[19] J.G.S. Van Jaarsveld, J.S.J. Van Deventer, L. Lorenzen, The potential use of geopolymeric materials to immobilise toxic metals: Part I. Theory and applications, Miner. Eng. 10 (1997) 659–669.
[20] A. Palomo, M. Palacios, Alkali-activated cementitious materials: alternative matrices for the immobilisation of hazardous wastes: Part II. Stabilisation of chromium and lead, Cem. Concr. Res. 33 (2003) 289–295.
[21] Z. Yunsheng, S. Wei, C. Qianli, C. Lin, Synthesis and heavy metal immobilization behaviors of slag based geopolymer, J. Hazard. Mater. 143 (2007) 206–213.
[22] D.S. Perera, Z. Aly, E.R. Vance, M. Mizumo, Immobilization of Pb in a geopolymer matrix, J. Am. Ceram. Soc. 88 (2005) 2586–2588.
[23] D.S. Kosson, H.A. van der Sloot, F. Sanchez, A.C. Garrabrants, An integrated framework for evaluating leaching in waste management and utilization of secondary materials, Environ. Eng. Sci. 19 (2002) 159–204.
[24] ASTMC618-01, Standard specification for coal fly ash and raw or calcined natural pozzolan for use as a mineral admixture in concrete, in: Concrete and Aggregates, ASTM Book of Standards, October 2008.
[25] R.A. Fletcher, K.J.D. MacKenzie, C.L. Nicholson, S. Shimada, The composition range of aluminosilicate geopolymers, J. Eur. Ceram. Soc. 25 (2005) 1471–1477.
[26] C. Panagiotopoulou, E. Kontori, T. Perraki, G. Kakali, Dissolution of aluminosilicate minerals and by-products in alkaline media, J. Mater. Sci. 42 (2007) 2967–2973.
[27] D. Panias, I.P. Giannopoulou, T. Perraki, Effect of synthesis parameters on the mechanical properties of fly ash-based geopolymers, Colloid Surface A 301 (2007) 246–254.

[28] H.Y. Ghorab, S.H.A.E. Fetouh, Factors affecting the solubility of gypsum: II. Effect of sodium hydroxide under various conditions, J. Chem. Technol. Biotechnol. 35 (1985) 36–40.
[29] T. Bakharev, Geopolymeric materials prepared using Class F fly ash and elevated temperature curing, Cem. Concr. Res. 35 (2005) 1224–1232.
[30] A. Palomo, M.W. Grutzeck, M.T. Blanco, Alkali-activated fly ashes: a cement for the future, Cem. Concr. Res. 29 (1999) 1323–1329.
[31] M. Criado, A. Fernández-Jiménez, A. Palomo, Alkali activation of fly ash: effect of the SiO_2/Na_2O ratio: Part I: FTIR study, Micropor. Mesopor. Mater. 106 (2007) 180–191.
[32] A. Fernández-Jiménez, A. Palomo, Mid-infrared spectroscopic studies of alkali-activated fly ash structure, Micropor. Mesopor. Mater. 86 (2005) 207–214.
[33] W.K.W. Lee, J.S.J. van Deventer, Structural reorganisation of class F fly ash in alkaline silicate solutions, Colloid Surface A 211 (2002) 49–66.
[34] S.N. Ghosh, Infra-red spectra of some selected minerals, rocks and products, J. Mater. Sci. 13 (1978) 1877–1886.
[35] V.C. Farmer, The Infrared Spectra of Minerals, Mineralogical Society, London, 1974.
[36] E. Dowty, Vibrational interactions of tetrahedra in silicate glasses and crystals – II. Calculations on melities, pyroxenes, silica polymorphs and feldspars, Phys. Chem. Miner. 14 (1987) 122–138.
[37] G. Socrates, Infrared and Raman Characteristic Group Frequencies, 3rd ed., John Wiley & Sons Ltd., England, 2001.
[38] T. Isobe, M. Senna, Control of litharge-massicot transformation by doping and mechanical activation, React. Solid 8 (1990) 29–40.
[39] A. Raman, B. Kuban, A. Razvan, The application of infrared spectroscopy to the study of atmospheric rust systems—I. Standard spectra and illustrative applications to identify rust phases in natural atmospheric corrosion products, Corros. Sci. 32 (1991) 1295–1306.
[40] T. Tsujimura, X. Xue, M. Kanzaki, M.J. Walter, Sulfur speciation and network structural changes in sodium silicate glasses: constraints from NMR and Raman spectroscopy, Geochim. Cosmochim. Acta 68 (2004) 5081–5101.
[41] C. Isabella, G.C. Lukey, H. Xu, J.S.J. Van Deventer, The effect of aggregate particle size on formation of geopolymeric gel, in: CD-ROM Proceedings of International Conference on Advanced Materials for Construction of Bridges, Buildings and other Structures-III, Davos, Switzerland, 2003.
[42] C. Fernández Pereira, Y. Luna, X. Querol, D. Antenucci, J. Vale, Waste stabilization/solidification of an electric arc furnace dust using fly ash-based geopolymers, Fuel 88 (2009) 1185–1193.
[43] J.G.S. van Jaarsveld, J.S.J. van Deventer, The effect of metal contaminants on the formation and properties of waste-based geopolymers, Cem. Concr. Res. 29 (1999) 1189–1200.
[44] M. Izquierdo, X. Querol, J. Davidovits, D. Antenucci, H. Nugteren, C. Fernández-Pereira, Coal fly ash-slag-based geopolymers: microstructure and metal leaching, J. Hazard. Mater. 166 (2009) 561–566.
[45] F.M.F. Santos, P.S. Pina, R. Porcaro, V.A. Oliveira, C.A. Silva, V.A. Leão, The kinetics of zinc silicate leaching in sodium hydroxide, Hydrometallurgy 102 (2010) 43–49.
[46] A. Fernández-Jiménez, A. Palomo, D.E. Macphee, E.E. Lachowski, Fixing arsenic in alkali-activated cementitious matrices, J. Am. Ceram. Soc. 88 (2005) 1122–1126.
[47] J.W. Phair, J.S.J. van Deventer, J.D. Smith, Effect of Al source and alkali activation on Pb and Cu immobilisation in fly-ash based geopolymers, Appl. Geochem. 19 (2004) 423–434.